DOI: 10.13009/EUCASS2019-917

Microwave processing of regolith – a 1D-printing cavity for enabling lunar construction technology

Lucas Thiébaut and Aidan Cowley***
** European Astronaut Centre EAC, European Space Agency, Linder Höhe, 51170 Köln, Germany*
lucas1.thiebaut@gmail.com
*** European Astronaut Centre EAC, European Space Agency, Linder Höhe, 51170 Köln, Germany*
aidan.cowley@esa.int

Abstract
A newly imagined 1D-Printing concept for regolith is depicted in this paper. The effects of microwaves on lunar soil are macroscopically described and a discussion on the mimicking of the dielectric and magnetic properties of lunar regolith microscopically using simulant is made. COMSOL Multiphysics microwave heating simulations have been run to theoretically test the concept using physical properties of regolith found in literature.

1. Introduction

Accessing space resources via in-situ resources utilization (ISRU) is increasingly an important part of research focused on a sustainable return to the moon. The Spaceship EAC initiative launched by the European Space Agency (ESA) and based at the European Astronaut Centre (EAC) has developed its capabilities in this field over the last number of years, in collaboration with a variety of research institutes, and is focusing part of its ISRU studies on the microwave (MW) processing of regolith. Inspiration is also drawn from the context of the moon village and in the light of building a lunar base using additive manufacturing (AM) where regolith as is used as a construction material. Techniques include using regolith simulants and additives such as binding polymer to 3D-print structures [1] and others aim at using raw regolith alone with a heating source such as laser [2], solar concentration [3] and microwaving [4]. The objective is to transform the powder into a compact building material (i.e. densification), by either molten lunar soil extrusion, direct energy deposition, powder bed fusion or powder bed sintering [5]. Inspiration for a lunar base is readily taken from previous ESA studies in collaboration with Foster & Partners (Figure 1), where the aim would be to create a thick regolith protective layer on top of an inflatable dome. The major advantages of using MW processing over other more conventional methods are its energy efficiency [6], [7] and its potential for the building of large structures. The enhancement of this technique is supported by the hope of new improvements in the field that could be used for other processes in terrestrial industries as well [7], and be applicable as an enabler of other ISRU processes.

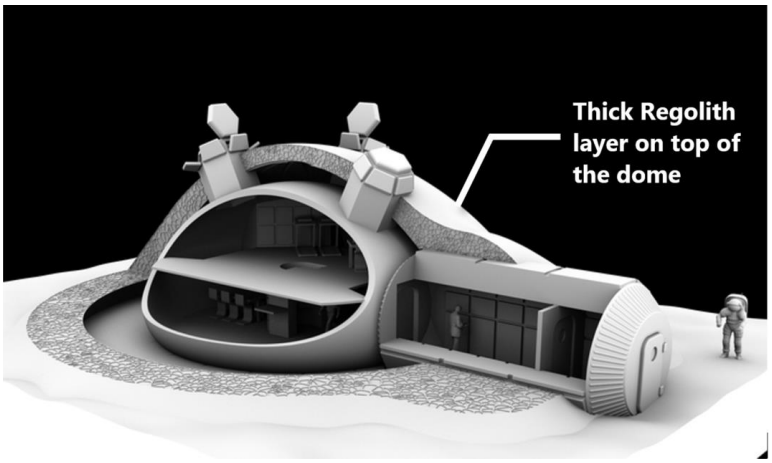

Figure 1: Lunar base envisioned together by ESA and Foster + Partners [8]

DOI: 10.13009/EUCASS2019-917

2. 1D-Printing microwave cavity concept

AM with microwaves remains a technically challenging development. In order to advance this objective, the development of a test set-up to demonstrate the 1D-Printing of a regolith brick using the inhomogeneity of a 2.45 GHz (1000W) electromagnetic (EM) field in a metallic cavity is currently ongoing. Melting and sintering of lunar regolith and simulant with this MW frequency has already been shown multiple times by different authors [4], [9]–[11] and previously by the Spaceship EAC team [12].

The concept of a 1D-Printing cavity comes from the fact that during microwave heating in a multimode cavity (microwave oven), it is unlikely to achieve perfect homogeneity of the electromagnetic field repartition. Indeed, constructive and destructive interferences are creating resonances of the waves inside the cavity after emission from the MW emitting device (i.e. magnetron) [13]. The creation of a subsequent three-dimensional standing wave with a high repartition of EM field amplitudes is then observed in the chamber. The regions where the wave amplitude is the highest are colloquially known as hot spots, and reciprocally cold spots are the regions where the amplitude is the lowest. This phenomenon is illustrated with the electric field strength values in Figure 2. The presence of these hot spots when a material is being heated in a microwave cavity will lead to local heating runaways inside the processed material [14]. Hence, during MW processing, this hot spot creation is viewed as major problem since it produces temperature gradients inside the material, which are responsible of local stresses and sometimes cracking [15]. However, hot spots can also be desirable to some extent [16] and this is precisely the case in the 1D-Printing concept.

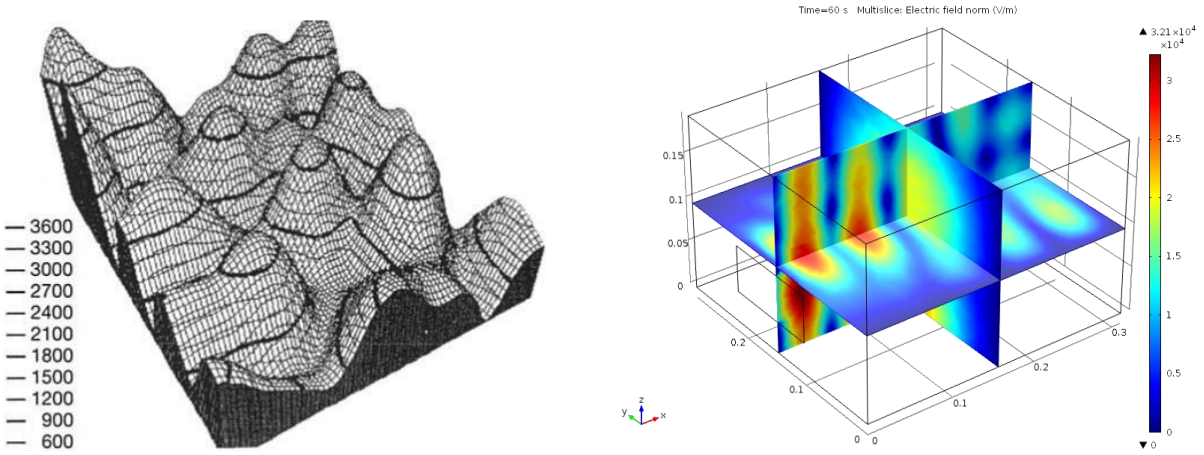

Figure 2: Electric field strength (left) at height z = 3.5 cm inside a MW oven [14]; (right) in a 31.1×29.3×19.5 cm cavity with a 11.3×5.2 cm TE10 2.45 GHz port in COMSOL Multiphysics 4.4

The idea is to place the material (i.e. regolith) into a 12.4×3.1× 2.6 cm alumina crucible, itself placed into a MW kiln. The kiln is lying on alumina rods, themselves transparent to microwaves at ambient temperature [17] and can be moved to the right or to the left since the rods are held by a moving metallic panel as shown in Figure 3 on the left. This whole system can be implemented within a microwave cavity by making sure that no substantial MW leakage is allowed. This enables a movement of the kiln inside the cavity within the x-axis. An example with a modified microwave oven is demonstrated on Figure 3 on the right. The interior of the kiln is covered by silicon carbide (SiC) susceptor powder layer which enable hybrid microwave heating (HMH), or direct microwave heating (DMH) if removed [17], [18].

Once the magnetron is running and the microwaves are emitted in the cavity, hot spots will soon be formed. Straightaway, MW will penetrate the materials and specific spots of the regolith should heat up more quickly than others, some reaching sintering/melting temperature after several minutes (empirically observed). Theoretically, if the kiln is moved inside the cavity, the EM field pattern should be impacted [14] and hot spots with new locations should be created. Then the regolith should be rapidly heated in new locations as well and potentially enable powder bed fusion/sintering of a first layer for a regolith brick.

DOI: 10.13009/EUCASS2019-917

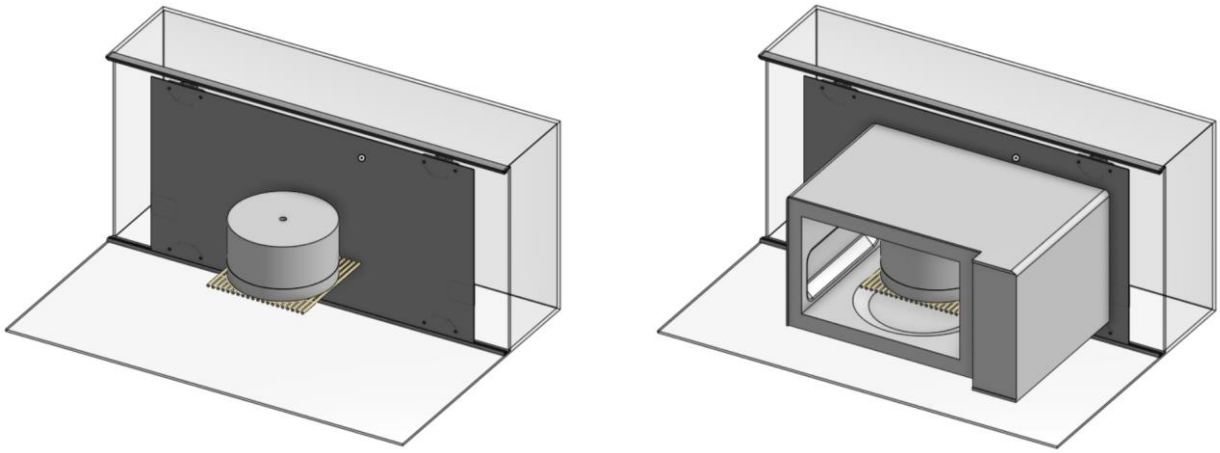

Figure 3: CAD model of (left) the moving panel (x-axis) with the kiln on top of the alumina rods; (right) the system installed behind an altered microwave oven (door not represented)

3. Effect of microwaves on regolith

The heating of regolith using microwaves has been introduced in the previous section but the mechanisms of this electromagnetic energy conversion into heat are described more in detail in this section.

3.1 Wave penetration and absorption in the material

At a macroscopic level, the microwave processing of materials in general is ruled by their dielectric and magnetic properties. The interactions between the electrical and magnetic field with a material is given by the permittivity ε (F/m) and the permeability μ (H/m) of the material, following equations (1) and (2) [19]:

$$\vec{D} = \varepsilon \vec{E} \quad \textbf{(1)}$$

$$\vec{B} = \mu \vec{H} \quad \textbf{(2)}$$

With $\vec{E}$ the electric field (V/m), $\vec{H}$ the magnetic field (A/m), $\vec{D}$ the electric flux density (Coul/m^2) and $\vec{B}$ the magnetic flux density (Wb/m^2). The permittivity and permeability can be given under a matrix form in the case of an anisotropic material or as a single value for an isotropic material. These properties can be written under a complex form and a relative form by diving them by their free space values following equations (3) and (4) [17]–[19]:

$$\varepsilon = \varepsilon_0 \varepsilon_r = \varepsilon' - i\varepsilon'' = \varepsilon_0(\varepsilon_r' - i\varepsilon_r'') \quad \textbf{(3)}$$

$$\mu = \mu_0 \mu_r = \mu' - i\mu'' = \mu_0(\mu_r' - i\mu_r'') \quad \textbf{(4)}$$

With $\varepsilon_0 = 8.854 \times 10^{-12}\ F/m$ the free space permittivity, $\mu_0 = 4\pi \times 10^{-7} H/m$ the free space permeability, ε_r and μ_r the relative permittivity and permeability, respectively. The real part of each equation (ε_r', μ_r') is referring to the energy storage capability whereas the imaginary part (ε_r'', μ_r'') is indicating the ability to dissipate the energy, mainly into heat. Two main mechanisms of MW absorption can then be dissociated considering whether the electrical or magnetic field absorption [16]. These are called the dielectric absorption and the magnetic absorption. A direct impression of this absorption can be given by the loss tangent values calculated with equations (5) and (6) [17].

$$\tan\delta_e = \frac{\varepsilon''}{\varepsilon'} = \frac{\varepsilon_r''}{\varepsilon_r'} \quad \textbf{(5)}$$

$$\tan\delta_m = \frac{\mu''}{\mu'} = \frac{\mu_r''}{\mu_r'} \quad \textbf{(6)}$$

DOI: 10.13009/EUCASS2019-917

With $\tan\delta_e$ the dielectric tangent loss and $\tan\delta_m$ the magnetic tangent loss, both dimensionless. Consequently, the penetration depth, which is the distance at which the intensity of the wave in the material is reduced to e^{-1} (36.8%) of its intensity at the surface, is given by equation (7) [16], [17]:

$$d_p = \frac{c}{\sqrt{2}\pi f\sqrt{\mu'_r\varepsilon'_r}}\left[(1+\tan^2\delta_e\tan^2\delta_m+\tan^2\delta_e+\tan^2\delta_m)^{\frac{1}{2}}+\tan\delta_e\tan\delta_m-1\right]^{-\frac{1}{2}} \quad \textbf{(7)}$$

With $c = \frac{1}{\sqrt{\varepsilon_0\mu_0}} = 3\times10^8\ m/s$ the light velocity and f the frequency of the wave. In the case of conductive material, the penetration depth can be obtained using the skin depth value of equation (8) [17], [18]:

$$d_p = \delta = \sqrt{\frac{1}{\pi f\mu\sigma_e}} \quad \textbf{(8)}$$

The dielectric absorption (or loss) is the main principle of electrically insulating materials heating using MW. It happens through the relaxation of polarized molecules or particles. In the case of 2.45 GHz microwaves, the predominant polarization loss is due to dipole relaxation. Indeed, other polarization effects such as ionic, electronic or interfacial polarization can happen at higher or lower frequencies but are not important enough here to have a major impact [17], [20], [21]. In materials containing free charge carriers such as regolith, this loss is also induced by conduction loss since the varying electrical field creates a movement of these charges, causing heating by resistance/Joule effect [16]. The conduction loss is taken into account by adding an extra term containing the conductivity normalized by the angular frequency in an effective imaginary part of the permittivity [17], [22].

The magnetic absorption is due to either eddy current loss, hysteresis loss or so-called residual loss such as magnetic resonance loss and domain wall oscillations [16] , [22]. The focus of interest in this work is on the two first mechanisms. The first one is caused by the induction of close loops electrical current in the material by the alternating magnetic field, leading to Joule heating. The second one is linked to the magnetic dipoles relaxation during oscillation, which is causing friction and heating when the magnetization of the material is following a hysteresis. This later mechanism should however stopping above the Curie temperature [16].

The volumetric power P_v dissipated in W/m^3 can then be calculated using equation (9) considering the two aspects.

$$P_v = \pi f(\mu_0\mu''_r H^2 + \varepsilon_0\varepsilon''_r E^2) \quad \textbf{(9)}$$

3.2 Discussion on mimicking lunar regolith properties with simulant

Mimicking perfectly the dielectric and magnetic properties of lunar regolith with terrestrial minerals is complicated and can be onerous. On the one hand because the lunar soil components cannot all be replicated and on the other hand because absorption stays stochastic and produces a high variability in the results. A strong emphasis has also to be made on the high regolith composition dispersion over the moon surface [23]–[25]. Nonetheless, concerning the dielectric properties, the relative permittivity of the simulant JSC-1A/2A has been shown to be comparable with the one of mare lunar regolith at ambient temperature amongst different simulant produced in the US [26], [27].

Lunar regolith being a mix between paramagnetic, ferromagnetic [28], antiferromagnetic [29], [30], semiconductor and conductor materials [10], the magnetic comportment is largely dependent on various contributions. These contributions are not only based on the mineralogical composition in itself but also on the physical aspects of the powder such as the grain size [30] and shape [31] and interactions between different structures such as oxide layers and iron particles [22]. Nonetheless, the major contribution to the magnetic properties of lunar regolith is still considered as coming from ubiquitous native nanophase iron (np-Fe^0) in agglutinic glass for low fields [10], [29], [32]. Single domain np-Fe^0 (grain size between 4 and 33 nm [24]) would be responsible for the Curie temperature of Apollo 11 fines found around 780°C for a 1.5 kHz magnetic field [29] and for a Curie point of 775±10°C for Apollo 11, 12, 14 and 16 samples for a 9.1 GHz field [32]. Indeed, the measurements of the reversible susceptibility for the Apollo 11 fines show no real disturbance before 780°C and it was concluded that the ilmenite/magnetite interaction with the

DOI: 10.13009/EUCASS2019-917

magnetic field would be negligible and the magnetic susceptibility was driven by the superparamagnetic iron particles [29], [32]. The mechanism of absorption of these particles is apparently mostly relying on eddy current loss following Zhang et al. (2010) [21] who worked on Fe/TiO_2 composites with amorphous TiO_2 and Fe grain of 17 mm size. This is also underlined by Liu et al. (2016) but for another metal-ceramic system Ti/SiO_2 and bigger grain size [33]**.** Galek (2013) [22] has as well described eddy currents induction as a major factor of magnetic heating of conductive and ferromagnetic materials. However in the case of regolith simulant, the properties are mainly governed by oxides such as magnetite, and thus by magnetic-hysteresis loss with a Curie point situated around 580°C [32].

JSC-1A has also been shown to be the simulant with the real and imaginary permeability properties the closest to the ones of mare lunar regolith at ambient temperature [26]. This would be due to the presence of nanophase-sized Ti-magnetite in this material [34]**.** The magnetic heating of magnetite is apparently still persisting above Curie temperature, just as the eddy current induction would do for the np-Fe^0, due to electron spin interactions [22]. So even though there is no largely distributed simulant containing those native iron particles, and that **s**imulants with np-Fe^0 have been successfully produced by different methods [35], [36], there would be no point of putting so much efforts in modifying JSC-1A for microwave heating applications [34]. In this logic, JSC-2A is chosen as the simulant to replicate lunar regolith in microwave processing experiments. However, a question arises about the reliability of simulant behaviour at higher temperatures.

4. Modelling of regolith properties

Simulations are made using the finite element modelling (FEM) software COMSOL Multiphysics version 4.4 to theoretically validate the cavity concept. Due to the aforementioned complexity of the regolith material and the lack of data about the high temperature behaviour of regolith properties, for both lunar regolith and simulant, assumptions are to be made to realise the models. The application of these models completed by other theoretical and empirical inputs will then be of great importance to have an insight of the real behaviour of regolith during microwave heating. JSC-2A being the simulant that would be employed for experimentation, a focus will be made on Low-Titanium Mare regolith for the simulations. The properties are modelled from ambient temperature (298 K) to temperatures below the regolith melting temperature considered equal to 1150°C (1423 K) [37]. The phase transformation and the molten state are not considered here.

4.1 Density

The regolith powder density is far from being constant and is subject to a lot of fluctuation depending on the location on the moon, the depth and other criteria. The wide range of densities going from roughly 1.4 g/cm^3 to 1.9 g/cm^3 [38] gives a wide range of thermal properties since most of them are related [24]. The thermal conductivity [39], the heat capacity [24], dielectric properties [25] and potentially the permeability are all dependent on the bulk density.

The thermodynamic conditions such as temperature and pressure have a substantial impact on the density. The density depends on the holding duration of the material at a certain temperature and pressure in the case of powders (i.e. sintering) and rapid heating such as microwave heating does not necessarily give enough time for the system to stabilise its properties. The density evolution of regolith during microwave processing is then very difficult to model and will therefore be considered as a constant before melting temperature throughout the simulations.

Loose regolith has an estimated average bulk density of 1.66 ± 0.05 g/cm^3 considering the first 60 cm of depth on the moon [24]. Considering the density measurement of JSC-1A regolith simulant when no pressure was applied on the powder, an average density of 1.65 g/cm^3 is obtained, the true density of the simulant being 2.90 g/cm^3 [26], [31], [40]. The mean values for simulant and lunar soil are then close and a bulk density of 1650 kg/m^3 has been selected for the model.

4.2 Electrical conductivity

At ambient temperature, lunar dust has a very low electrical conductivity [24]. This conductivity is believed to be predominantly controlled by ionic conduction and semiconducting mechanisms in absence of moisture which gives a high temperature dependency of the phenomena [41]. Schreiner et al. (2016) [23] used the electrical conductivity data from Apollo samples, basalt rocks and oxides mix powder to fit it with of Vogel-Tamman-Fulcher equation to gives its evolution with temperature increase. This type of equation is frequently used for the modelling of conductivity variation with temperature for ceramic materials [42]. For Mare regolith, the regression coefficients are given in equation (10).

DOI: 10.13009/EUCASS2019-917

$$\sigma_e = 3.130 \times 10^4 \exp\left(\frac{-1.154 \times 10^4}{T}\right) \quad \textbf{(10)}$$

With σ_e the electrical conductivity in S/m, T the temperature in K. The previous version of the equation is containing T_g, the glass transition temperature in K, which should be put to zero at low temperature to avoid vertical asymptotes [23]. The domain before melting temperature is considered as a low temperature domain, therefore T_g is set to zero. The evolution of σ_e with T is given on Figure 4. To avoid calculations errors due to precision in COMSOL, the conductivity is fixed to the lower positive constant value superior to zero available on the software (called "eps") below 700 K.

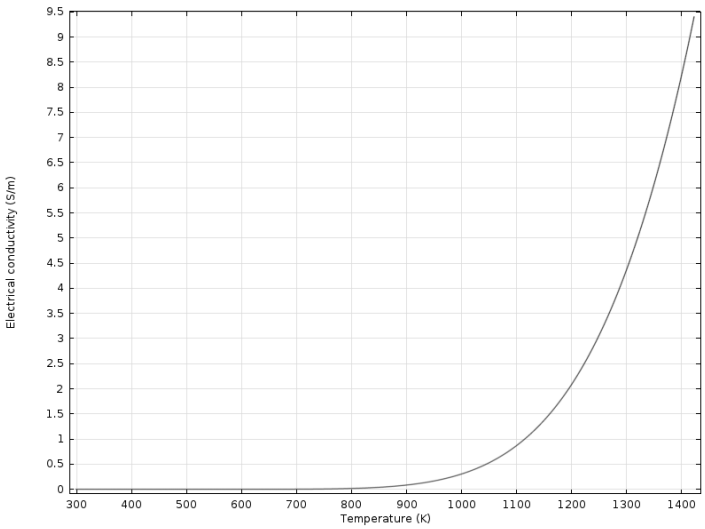

Figure 4: Electrical conductivity in function of temperature, modelling on COMSOL for Low-Titanium Mare regolith from ambient temperature to melting temperature

4.3 Thermal conductivity

The low thermal conductivity of regolith has a major impact on the creation of temperature gradients inside the material during microwave heating which would lead to internal heat stress during absorption [43]. Measurements of thermal conductivity of regolith from Apollo samples have only been made for temperatures below 500 K. Therefore, the model proposed by Schreiner et al. (2016) [23] uses the data from oxides mix and FJS-1 simulant to a fitting function given by equation (11). The plot for this equation is given on Figure 5.

$$k = \frac{0.01257\left(\frac{T - 691.7}{564.3}\right) + 0.0172}{\left(\frac{T - 691.7}{564.3}\right)^2 - 2.874\left(\frac{T - 691.7}{564.3}\right) + 2.085} \quad \textbf{(11)}$$

Here, k the thermal conductivity, is in W/(m·K). Another approximation of the thermal conductivity evolution with temperature had been made by Colozza (1991) [44] for granular regolith. This other model shows a different behaviour after melting temperature, where k tends to increase at a certain point. This difference of feature will not have any impact on our simulation since the model is kept under regolith melting temperature.

4.4 Heat capacity at constant pressure

The specific heat of regolith before melting temperature is also based on the model of Schreiner et al. (2016) [1]. For temperature understood between 90 and 350 K, the heat capacity can be approximated by equation (12) from Hemingway et al. (1974) [45] considering that the values for Highland, Mare regolith and simulant are in the same neighbourhood for these low values of temperature. With C_p the heat capacity at constant pressure in J/(kg·K). Above 350 K and until melting temperature the model uses values calculated using a method from Stebbins et al. (1984) [46].

DOI: 10.13009/EUCASS2019-917

This model is a prediction employing the mole faction of the oxide components for silicate glasses for temperatures of roughly 400-1000 K. Specific values are given for Low-Ti Mare regolith in equation (13).

$$C_p(T) = -2.32 \times 10^{-2} + 2.13 \times 10^{-3}T + 1.50 \times 10^{-5}T^2 - 7.37 \times 10^{-8}T^3 + 9.66 \times 10^{-11}T^4 \quad \textbf{(12)}$$

$$C_p(T) = 9.093 \times 10^{2} + 2.870 \times 10^{-1}T - 2.469 \times 10^{7}T^{-2} \quad \textbf{(13)}$$

A continuous first derivative smoothing is applied between the two functions to wipe the abrupt slope modification. Figure 6 shows the values of the specific heat as simulated on COMSOL.

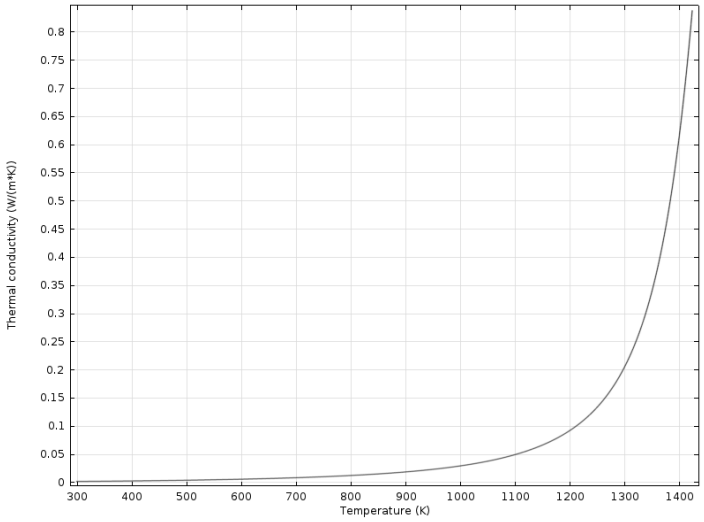

Figure 5: Thermal conductivity in function of temperature, modelling on COMSOL for Low-Titanium Mare regolith from ambient temperature to melting temperature

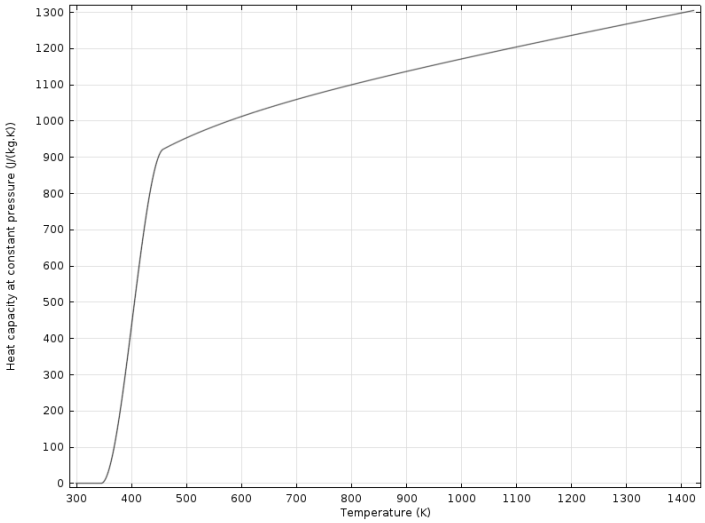

Figure 6: Heat capacity at constant pressure in function of temperature, modelling on COMSOL for Low-Titanium Mare regolith from ambient temperature to melting temperature

DOI: 10.13009/EUCASS2019-917

4.5 Relative permittivity

No empirical data about the behaviour of lunar soil permittivity above 100°C at the MW frequency of 2.45 GHz has been found. The only experimental permittivity measurements above 200°C for regolith at 2.45 GHz are from Allan et al. (2013) [9] and were made using pressed 264 mg weight and 2.09±0.15 g/cm^3 density JSC-1AC pellets in argon. The difference of density, grain size, the presence of adsorbed moisture [47] and other factors such as the grains shape [31] and measurement technique have an important effect on the permittivity behaviour at ambient temperature, as shown in Figure 7. With the heat creation by microwave absorption, these behavioural differences between lunar regolith and simulant might even be more pronounced. Moreover, the oxidation of regolith in air at high temperature will more than likely have an impact on the dielectric properties and this is not taken into account here.

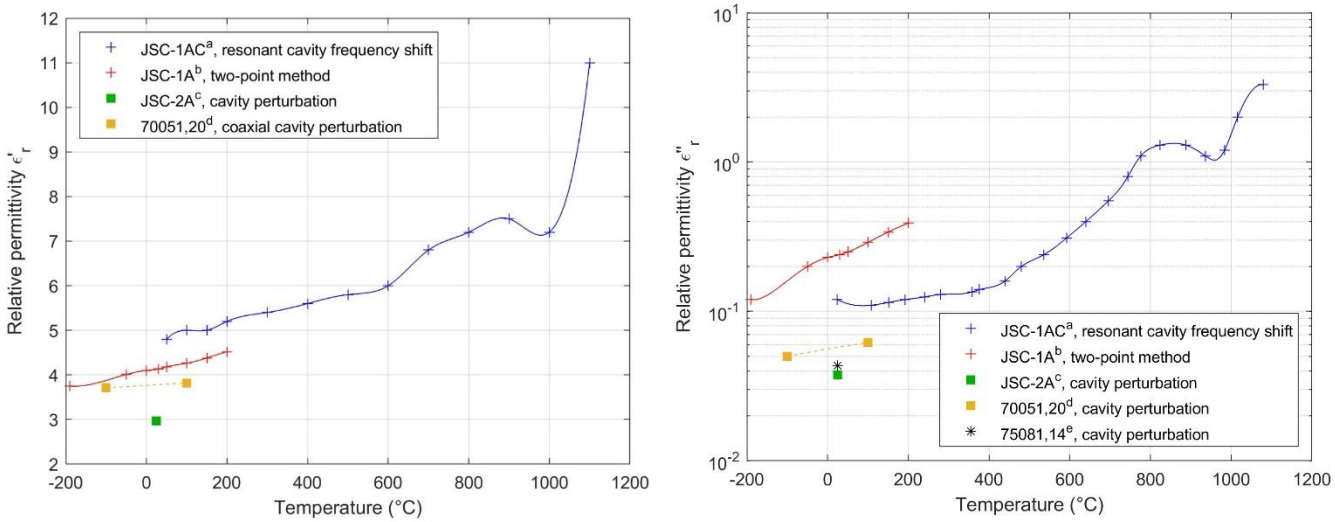

Figure 7: Real and imaginary relative permittivity of simulant and lunar regolith for different samples and different techniques of measurements. Ref: [a][9], frequency 2.45 GHz; [b][27], frequency 2.5 GHz; [c][31], frequency 2.161 GHz; [d][48], frequency 2.5 GHz; [e][49], frequency 2.45 GHz

Nevertheless, the input from Allan et al. (2013) will still be used for the microwave absorption modelling of regolith at high temperature since the natural dependency of the properties on many physical and chemical factors will prevent the finding of fixed values. This will at least give the general increasing behaviour of the permittivity and dependency on moisture evaporation/desorption, glass transition and hot crystallisation.

4.6 Relative permeability

Modelling the complex permeability of regolith is still a challenge. As discussed earlier, depending on the considered material, i.e. JSC-2A simulant or lunar regolith itself, the magnetic comportment is not based on the same elements. In addition, depending on the elements responsible of the permeability, the behaviour with temperature would not necessarily be the same. The magnetic loss values from Barmatz et al. [26], [31], [49] should not be enough to truly describe this behaviour since they are measured at ambient temperature and the mechanisms responsible of these losses are yet unsure. For instance, as the magnetic heating of regolith seems governed by eddy currents formation in the native iron particles present in agglutinic glass, conductivity modifications, linked to temperature change, should have an impact on the magnetic absorption, meaning the permeability.

However, due to the intricacy aforementioned, values, which are constant with temperature, will again be chosen using the given scientific data. The real part of the permeability is considered equal to 1 since values close to this have been mainly reported [31], [49], [50]. An arbitrary value of 0.02 has been selected for the imaginary part, based on [31]. To check the importance of these values in the modelling, a permeability of $1.05 - j \times 0.05$ based on [49] has also been tried but does not show great changes in the magnetic heating results.

DOI: 10.13009/EUCASS2019-917

5. Simulations

5.1 Model description

The empirical appreciation of the high temperatures reached by the regolith during microwave heating has been used to build a 2D cut view model of the Figure 2 (right) system. It consists in a 50×30 cm cavity with a 1 kW TE1 MW input port of 8cm long placed in the centre of the right side of the cavity as can be seen on Figure 8. Inside the cavity, the kiln laying on the alumina rods contains an alumina crucible filled on 1.5 cm height with regolith. A fine physic-controlled mesh is being used. The model is considered as running in atmosphere, the cavity is hence filled with air. A parameter a in meter is used to determine where on the x-axis the kiln is placed. When a is equal to 0, the kiln is in the centre of the cavity. Positive a is a displacement on the right and negative a a displacement on the left. The susceptor layer can be removed to make the model run in HMH or DMH.

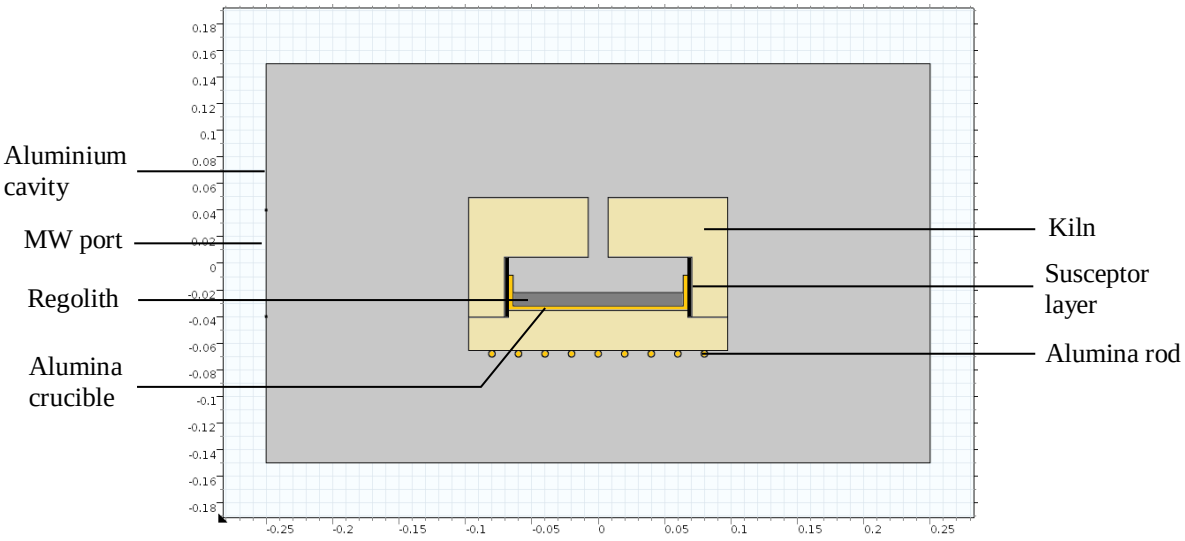

Figure 8: Geometry of the model on COMSOL Multiphysics, a=0 m

5.2 System materials modelling

Since regolith is not the only material in the cavity that can be submitted to interaction with the electromagnetic waves in our model, it is important to take into account the properties evolution of the kiln and the crucible as well. The permittivity properties of the alumina rods and the alumina crucible are based on the measurements made by Greenacre (1996) [42] and the ones for the silicon carbide susceptor are read from Baeraky (2002) [51]. The polytype of SiC has a negligible impact on the permittivity [52].

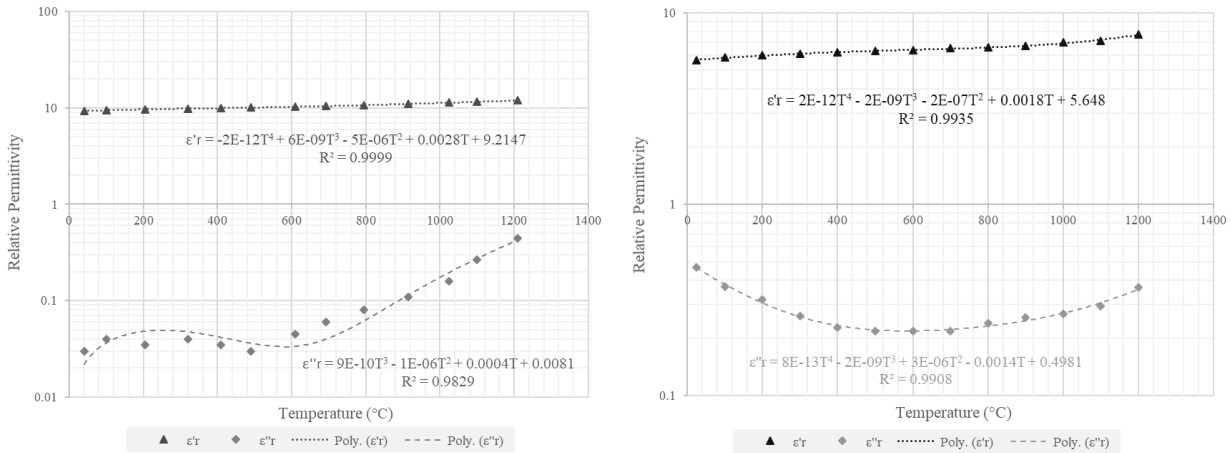

Figure 9: Evolution with temperature of the real and imaginary relative permittivity of (left) Alumina, data read from [42]; (right) Silicon carbide, data read from [51]

DOI: 10.13009/EUCASS2019-917

These data are fitted by third or fourth degrees polynomial functions, as shown on Figure 9, to be used on COMSOL. The rest of the properties for alumina are taken from [53] and a distinction is made with the kiln brick using thermal conductivity for a 15.2% porosity alumina foam [54] and a lower density. The electrical conductivity of SiC is based on [55] and the rest of the properties are defined in the COMSOL database.

5.2 Results and discussion

Computation have been made in the case of HMH and DMH for a values ranging from -0.12 m to 0.12 m by step of 0.02 m. The main results that can be observed for each simulation are that EM field hot spots are formed in all cases and the highest temperature increase rate tends to be at the same location than where hot spots are created when the time is equal to 0 min. This effect can be remarked on Figure 10 where a 1262 K hot spot is present at 35 min at the same location than the EM hot spot at 0 min. The kiln plays his role of insulator since the air outside of it remains close to ambient temperature.

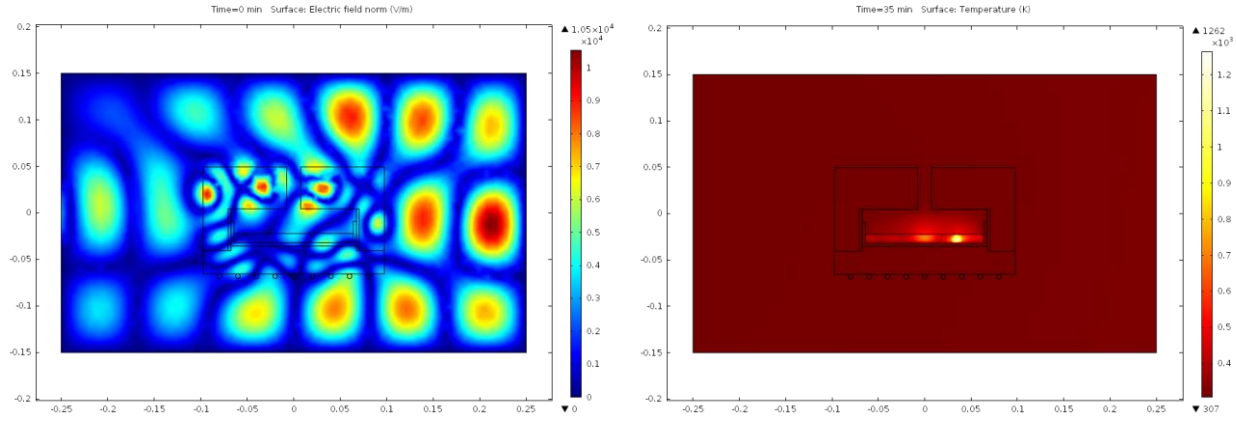

Figure 10: COMSOL Multiphysics simulation of (left) the electrical field distribution for a=0 m; (right) the temperature distribution for a=0.12 m

When the kiln is located in the centre of the cavity, the temperatures reached with HMH are much higher than with DMH (max. temperature of 433 K after 35 minutes), which shows that the presence of the susceptor is really helping the heating of the regolith. Moreover, the hot spots positions were found different. However, surprisingly, the regolith heating rate is found much higher without the presence of susceptor in the model for some values of a such as a=0.04 m where the powder is reaching a temperature of 1384 K after 10 minutes when HMH needs 35 minutes to reach 1388 K. This shows that although DMH can offer better results in terms of heating, the presence of susceptor stabilises the system giving a similar heating rate each time.

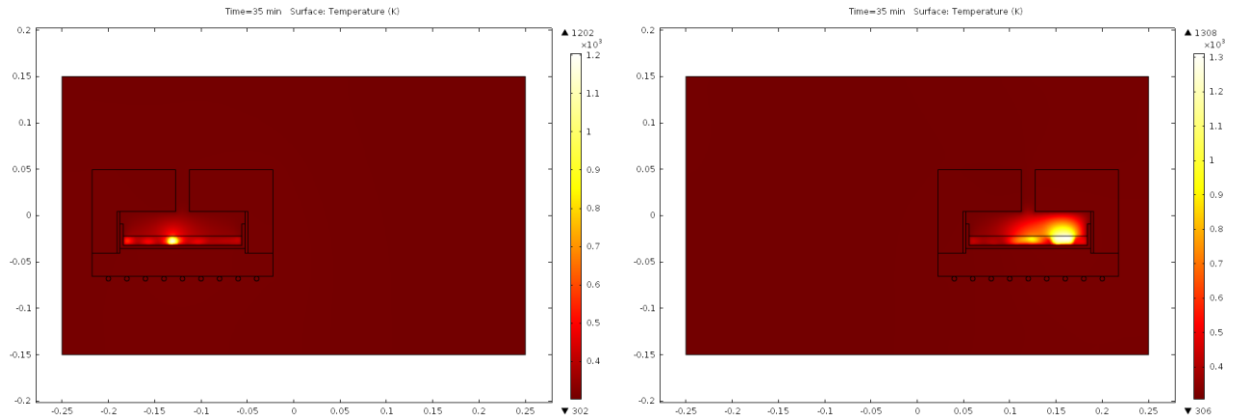

Figure 11: COMSOL Multiphysics simulation of temperature distribution in the case of hybrid microwave heating for (left) a=-0.12 m; (right) a=0.12 m

DOI: 10.13009/EUCASS2019-917

This stabilising effect of the susceptor [17] can be seen in the comparison of Figure 11 and Figure 12. In the HMH the temperature reached after 35 minutes is almost the same for two different values of a, whereas a greater disparity is present for DMH. Moreover, the heating patterns are not the same, with a different positioning of the hot spots. The presence of susceptor is changing the EM field resonance in the cavity, modifying the focusing of the waves inside the kiln. It is possible to notice the selective heating of microwaves since the susceptor is not absorbing MW as much as regolith is.

For almost all the values of a in HMH, the formation of a hot spot in the centre of the crucible was observed. This gives us the information that the kiln is acting as a resonant cavity itself, even though transparent to microwaves since the values of permittivity are greater than 1, and seems to focus the waves. This could lead to the idea that 1D-Printing is not feasible in the cavity as imagined. Nevertheless, some models such as a=12 on the right side of Figure 11 are showing an offset hot spot. The potential of the concept therefore still exists.

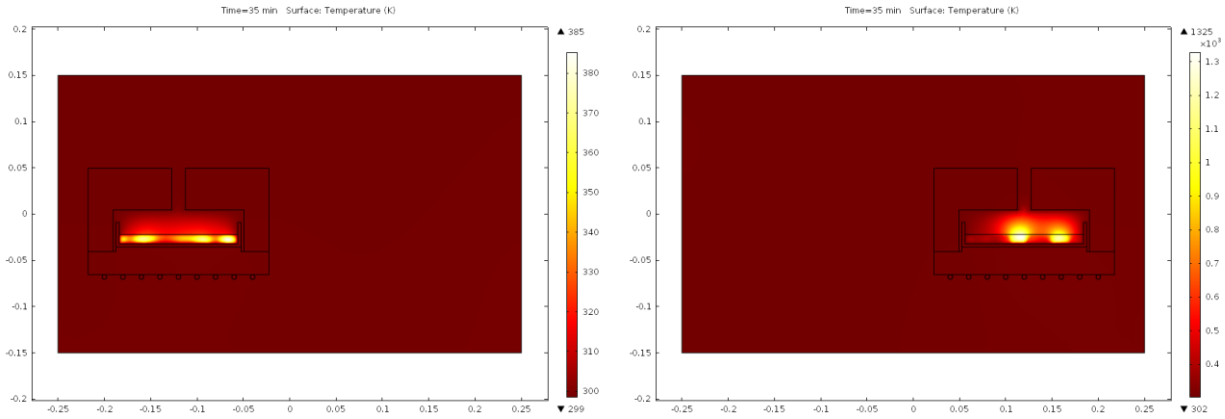

Figure 12: COMSOL Multiphysics simulation of temperature distribution in the case of direct microwave heating for (left) a=-0.12 m; (right) a=0.12 m

6. Conclusion and perspectives

The low technology readiness level of microwave processing of regolith remains one of the major problem in the development of new ways to achieve AM on the moon using ISRU. Even though the 1D-Printing concept seems to show some limitations such as the focusing of the waves in the centre of the sample by the kiln, an experimentation would be required to empirically certify the models. The significance of the COMSOL simulations is weakened if the fact that they remain in 2D is taken into account. Moreover, it does not show the stochastic variability of the results that have been observed previously [12]. Nonetheless, it stands as a new step in future improvements in this field and could greatly help for the design of another 1D-Printing cavity, 2D-Printing cavity, and even a molten extrusion mechanism.

DOI: 10.13009/EUCASS2019-917

References

[1] S. L. Taylor *et al.*, "Sintering of micro-trusses created by extrusion-3D-printing of lunar regolith inks," *Acta Astronaut.*, vol. 143, no. July 2017, pp. 1–8, 2018.

[2] N. Gerdes *et al.*, "Selective Laser Melting for processing of regolith in support of a lunar base," *J. Laser Appl.*, vol. 30, no. 3, p. 032018, 2018.

[3] B. Imhof *et al.*, "Advancing Solar Sintering for Building A Base On The Moon," *69 th Int. Astronaut. Congr.*, no. July 2018, pp. 25–29, 2017.

[4] M. Barmatz, D. Steinfeld, M. Anderson, and D. Winterhalter, "3D Microwave Print Head Approach for Processing Lunar and Mars Regolith," *45th Lunar and Planetary Science Conference*, pp. 3–4, 2014.

[5] T. D. Ngo, A. Kashani, G. Imbalzano, K. T. Q. Nguyen, and D. Hui, "Additive manufacturing (3D printing): A review of materials , methods , applications and challenges," *Compos. Part B*, vol. 143, no. February, pp. 172–196, 2018.

[6] M. Oghbaei and O. Mirzaee, "Microwave versus conventional sintering: A review of fundamentals, advantages and applications," *J. Alloys Compd.*, vol. 494, no. 1–2, pp. 175–189, 2010.

[7] S. Lim, V. L. Prabhu, M. Anand, and L. A. Taylor, "Extra-terrestrial construction processes – Advancements, opportunities and challenges," *Adv. Sp. Res.*, vol. 60, no. 7, pp. 1413–1429, 2017.

[8] ESA and Foster+Partners, "3D-Printed lunar base design," 2013. [Online]. Available: http://www.esa.int/spaceinimages/Images/2013/01/3D-printed_lunar_base_design.

[9] S. M. Allan, B. J. Merritt, B. F. Griffin, P. E. Hintze, and H. S. Shulman, "High-Temperature Microwave Dielectric Properties and Processing of JSC-1AC Lunar Simulant," *J. Aerosp. Eng.*, vol. 26, no. 4, pp. 874–881, 2013.

[10] L. A. Taylor and T. T. Meek, "Microwave Sintering of Lunar Soil: Properties, Theory, and Practice," *J. Aerosp. Eng.*, vol. 18, no. 3, pp. 188–196, 2005.

[11] T. T. Meek, D. T. Vaniman, R. D. Blake, and M. J. Godbole, "Sintering of Lunar Soil Simulants using 2.45 GHz Microwave Radiation," *Lunar Planet. Sci. Conf. XVIII*, no. January, pp. 635–636, 1987.

[12] T. Häfner, "A Microwave Sinter System for Lunar Regolith Studies", Master Thesis, 2015.

[13] S. Kamol, P. Limsuwan, and W. Onreabroy, "Three-dimensional standing waves in a microwave oven," vol. 78, no. 492, 2010.

[14] L. P. Kok and E. Boon, "The Problem of Hot Spots in Microwave Equipment Used for Preparatory Techniques-Theory and Practice," vol. 15, pp. 100–109, 1993.

[15] W. H. Sutton, *Microwave processing of materials*, vol. 18, no. 11. 1993.

[16] J. Sun, W. Wang, and Q. Yue, "Review on microwave-matter interaction fundamentals and efficient microwave-associated heating strategies," *Materials*, vol. 9, no. 4. 2016.

[17] M. Bhattacharya and T. Basak, "A review on the susceptor assisted microwave processing of materials," *Energy*, vol. 97, pp. 306–338, 2016.

[18] S. Singh, D. Gupta, V. Jain, and A. K. Sharma, "Microwave processing of materials and applications in manufacturing industries: A Review," *Mater. Manuf. Process.*, vol. 30, no. 1, pp. 1–29, 2015.

[19] D. M. Pozar, *Microwave Engineering*, 4th ed. 2012.

[20] M. Z. Firihu, I. N. Sudiana, and S. Mitsudo, "Microwaves enhanced sintering mechanisms in alumina ceramic sintering experiments," *Contemp. Eng. Sci.*, vol. 9, no. 5, pp. 237–247, 2016.

[21] Q. Zhang *et al.*, "Effect of metal grain size on multiple microwave resonances of Fe/ TiO 2 metal-semiconductor composite," *Appl. Phys. Lett.*, vol. 97, no. 13, 2010.

[22] T. Galek, "Modeling of Microwave Absorption Mechanisms in Metallic Powders," 2013.

[23] S. S. Schreiner, J. A. Dominguez, L. Sibille, and J. A. Hoffman, "Thermophysical property models for lunar regolith," *Adv. Sp. Res.*, vol. 57, no. 5, pp. 1209–1222, 2016.

[24] G. H. Heiken, D. T. Vaniman, and B. M. French, *Lunar Sourcebook: a user's guide to the moon*. 1991.

[25] G. R. Olhoeft and D. W. Strangway, "Dielectric properties of the first 100 meters of the Moon," *Earth Planet. Sci. Lett.*, vol. 24, no. 3, pp. 394–404, 1975.

[26] M. Barmatz *et al.*, "Microwave Permittivity and Permeability Measurements on Lunar Simulants," *Lunar Planet. Inst. Sci. Conf. Abstr.*, vol. 43, no. January 2016, p. 1050, 2012.

[27] O. P. N. Calla and I. S. Rathore, "Study of complex dielectric properties of lunar simulants and comparison with Apollo samples at microwave frequencies," *Adv. Sp. Res.*, vol. 50, no. 12, pp. 1607–1614, 2012.

[28] J. R. Bates and H. Kernaghan, "ALSEP Termination Report," no. April, 1979.

[29] S. K. Runcorn *et al.*, "Magnetic properties of Apollo 11 lunar samples," *Proc. Apollo 11 Lunar Sci. Conf.*, vol. 3, pp. 2369–2387, 1970.

[30] M. M. McElhinny, P. L. McFadden "Paleomagnetism Continents and Oceans" *Int. Geophys.*, vol. 73, no. C, 2000.

[31] M. Barmatz *et al.*, "Microwave Heating Studies and Instrumentation for Processing Lunar Regolith and

Simulants," *44th Lunar and Planetary Science Conference*, vol. 51, pp. 43–44, 2013.
[32] R. V Morris, R. V Gibbons, and F. Hörz, "FMR thermomagnetic studies up to 900°C of lunar soils and potential magnetic analogues," vol. 2, no. 10, pp. 2–5, 1975.
[33] W. Liu, F. Xu, Y. Li, X. Hu, B. Dong, and Y. Xiao, "Discussion on microwave-matter interaction mechanisms by in situ observation of 'core-shell' microstructure during microwave sintering," *Materials*, vol. 9, no. 3. 2016.
[34] L. A. Taylor, C. M. Pieters, and D. Britt, "Evaluations of lunar regolith simulants," *Planet. Space Sci.*, vol. 126, pp. 1–7, 2016.
[35] H. Tang, S. Wang, and X. Li, "Simulation of nanophase iron production in lunar space weathering," *Planet. Space Sci.*, vol. 60, no. 1, pp. 322–327, 2012.
[36] C. C. Hung, "Lunar dust simulant containing nanophase iron and method for making the same," 2012.
[37] A. Goulas, J. G. P. Binner, R. A. Harris, and R. J. Friel, "Assessing extraterrestrial regolith material simulants for in-situ resource utilisation based 3D printing," *Appl. Mater. Today*, vol. 6, pp. 54–61, 2017.
[38] J. H. Allton, C. Galindo Jr., and L. A. Watts, "Guide to using lunar soil and simulants for experimentation," 1985.
[39] C. Cremers, "Density, pressure and temperature effects on heat transfer in lunar material," vol. 9, no. 11, pp. 2180–2183, 1971.
[40] Z.-G. Yuan and J. Kleinhenz, "Measurement of Apparent Thermal Conductivity of JSC-1A Under Ambient Pressure," no. January 2011, pp. 1–12, 2012.
[41] G. R. Olhoeft, A. L. Frisillo, D. W. Strangway, and H. Sharpe, "Temperature dependence of electrical conductivity and lunar temperatures," *The Moon*, vol. 9, no. 1–2. pp. 79–87, 1974.
[42] Greenacre, "Measurement of the high temperature dielectric properties of ceramics at microwave frequencies," *Univ. Nottingham*, no. October, 1996.
[43] Q. Lu, "Caractérisation diélectrique de matériaux pulvérulents dans une large bande de fréquences micro-ondes," 2011.
[44] A. J. Colozza, "Analysis of lunar regolith thermal energy storage," *Nasa Cr*, no. 189073, p. 9p, 1991.
[45] B. S. Hemingway, R. A. Robie, and W. H. Wilson, "Specific heats of lunar soils, basalt, and breccias from Apollo 14, 15 and 16 landing sites, between 90 and 350 K," *Proc. fourth Lunar Sci. Conf.*, vol. 3, pp. 2481–2487, 1973.
[46] J. F. Stebbins, I. S. E. Carmichael, and L. K. Moret, "Heat capacities and entropies of silicate liquids and glasses," *Contrib. to Mineral. Petrol.*, vol. 86, no. 2, pp. 131–148, 1984.
[47] G. R. Olhoeft, D. W. Strangway, and A. L. Frisillo, "Lunar sample electrical properties."
[48] H. E. Bussey, "Dielectric Measurements of Lunar Soil," *Lunar Planet. Inst.*, pp. 1–3, 1978.
[49] M. Barmatz, D. Steinfeld, S. B. Begley, D. Winterhalter, and C. Allen, "Microwave permittivity and permeability measurements on lunar soils," *42nd Lunar and Planetary Science Conference*, pp. 4–5, 2011.
[50] J. Feng, Y. Su, C. Ding, S. Xing, S. Dai, and Y. Zou, "Dielectric properties estimation of the lunar regolith at CE-3 landing site using lunar penetrating radar data," *Icarus*, vol. 284, pp. 424–430, 2017.
[51] T. A. Baeraky, "Microwave Measurements of the Dielectric Properties of Silicon Carbide at High Temperature," *Egypt. J. Sol.*, vol. 25, no. 2, pp. 263–273, 2002.
[52] C. Raynaud, "Propriétés physiques et électroniques du carbure de silicium (SiC)," vol. 33, no. 0, 2007.
[53] P. Auerkari, "Mechanical and physical properties of engineering alumina ceramics," *VTT Tied. - Valt. Tek. Tutkimusk.*, no. 1792, 1996.
[54] T. Shimizu, K. Matsuura, H. Furue, and K. Matsuzak, "Thermal conductivity of high porosity alumina refractory bricks made by a slurry gelation and foaming method," *J. Eur. Ceram. Soc.*, vol. 33, no. 15–16, pp. 3429–3435, 2013.
[55] R. Heuguet, S. Marinel, A. Thuault, and A. Badev, "Effects of the susceptor dielectric properties on the microwave sintering of alumina," *J. Am. Ceram. Soc.*, vol. 96, no. 12, pp. 3728–3736, 2013.